The unique self-assembly/disassembly property of *Archaeoglobus fulgidus* ferritin and its implications on molecular release from the protein cage

Barindra Sana, Eric Johnson, Sierin Lim

PII: S0304-4165(15)00228-7
DOI: doi: 10.1016/j.bbagen.2015.08.019
Reference: BBAGEN 28270

To appear in: *BBA - General Subjects*

Received date: 8 April 2015
Revised date: 13 August 2015
Accepted date: 31 August 2015

Please cite this article as: Barindra Sana, Eric Johnson, Sierin Lim, The unique self-assembly/disassembly property of *Archaeoglobus fulgidus* ferritin and its implications on molecular release from the protein cage, *BBA - General Subjects* (2015), doi: 10.1016/j.bbagen.2015.08.019

The unique self-assembly/disassembly property of *Archaeoglobus fulgidus* ferritin and its implications on molecular release from the protein cage

Barindra Sana*, Eric Johnson†[§], and Sierin Lim*[1]

*School of Chemical & Biomedical Engineering, Division of Bioengineering, Nanyang Technological University, Singapore 637457

†Howard Hughes Medical Institute, Division of Chemistry and Chemical Engineering, California Institute of Technology, Pasadena, CA 91125, USA

[1]Correspondence to Sierin Lim, School of Chemical and Biomedical Engineering, Nanyang Technological University, 70 Nanyang Dr. Block N1.3, Singapore 637457, +65 6316 8966 (tel), SLim@ntu.edu.sg

[§]Present address: La Jolla Laboratories, Pfizer Worldwide Research & Development, San Diego, California 92121, USA.

Abstract:
BACKGROUND: In conventional in vitro encapsulation of molecular cargo, the multi-subunit ferritin protein cages are disassembled in extremely acidic pH and re-assembled in the presence of highly concentrated cargo materials, which results in poor yields due to the low-pH treatment. In contrast, *Archaeoglobus fulgidus* open-pore ferritin (AfFtn) and its closed-pore mutant (AfFtn-AA) are present as dimeric species in neutral buffers that self-assemble into cage-like structure upon addition of metal ions.

METHODS: To understand the iron-mediated self-assembly and ascorbate-mediated disassembly properties, we studied the iron binding and release profile of the AfFtn and AfFtn-AA, and the corresponding oligomerization of their subunits.

RESULTS: Fe^{2+} binding and conversion to Fe^{3+} triggered the self-assembly of cage-like structures from dimeric species of AfFtn and AfFtn-AA subunits, while disassembly was induced by dissolving the iron core with reducing agents. The closed-pore AfFtn-AA has identical iron binding kinetics but lower iron release rates when compared to AfFtn. While the iron binding rate is proportional to Fe^{2+} concentration, the iron release rate can be controlled by varying ascorbate concentrations.

CONCLUSION: The AfFtn and AfFtn-AA cages formed by iron mineralization could be disassembled by dissolving the iron core. The open-pores of AfFtn contribute to enhanced reductive iron release while the small channels located at the 3-fold symmetry axis (3-fold channels) are used for iron uptake.

GENERAL SIGNIFICANCE: The iron-mediated self-assembly/disassembly property of AfFtn offers a new set of molecular trigger for formation and dissociation of the protein cage, which can potentially regulate uptake and release of molecular cargo from protein cages.

Keywords: Protein cage, Self-assembly, Dissociation, Molecular release, Binding kinetics, Release kinetics

INTRODUCTION

Self-assembling protein cages have potential applications as molecular carriers and as templates for nanoparticle synthesis (*1-10*). Protein cages are formed by the self-assembly of multiple protein subunits into cage-like structures. Ferritins are multi-subunit protein molecules composed of 24 polypeptides that self-assemble into a hollow, roughly spherical protein cage having external and internal diameters of approximately 12 nm and 8 nm, respectively. Conversion of Fe^{2+} to Fe^{3+} is catalyzed by a ferroxidase center located within the hydrophilic interior of each subunit and iron core is formed by accumulation of Fe^{3+} at a nucleation site located within the cage. *In vivo*, the iron is stored as phosphate-conjugated ferrihydrite molecule while the exact chemical composition of the *in vitro* synthesized ferric core vary widely depending on the nature of ferritin molecule, proportion of iron loading, physical and chemical conditions of mineralization (*11-15*). In general, 3-fold and 4-fold channels (0.3-0.5 nm diameter) that connect the inner cavity to the ferritin surface are proposed as the route for inward and outward movement of iron, protons, and other molecules *in vivo* (*16, 17*). *In vitro* loading of larger molecules through these narrow channels has not been reported. To encapsulate large molecules, horse spleen ferritin has been disassembled into subunits at pH 2 and reassembled by increasing the pH in the presence of highly concentrated cargo materials (*18, 19*). However, this technique typically results in poor yields due to the irreversible changes of protein structure that occur at low pH. The oligomeric conformation of *Archaeoglobus fulgidus* ferritin (AfFtn) and its double mutant K150A, R151A (AfFtn-AA) can be manipulated through variation of ionic strength or by addition of specific metal ions (*20-24*). Previously we established the unique open cage structure of the wild-type AfFtn by X-ray crystallography and subsequently solved the crystal structure of the AfFtn-AA in a cannonical closed cage ferritin assembly (*20, 22*). Additional experiments demonstrated salt-mediated and metal-mediated self-assembly of the AfFtn and AfFtn-AA molecules under mild conditions, which are potentially advantageous for packaging molecular cargo within the protein cages. In low ionic strength buffers these ferritins are comprised of dimeric species that self-assemble into 24-meric cage-like structures as the buffer's ionic strength is increased. Self-assembly of dimeric AfFtn and AfFtn-AA into 24-mers could also be controlled by addition of ferrous iron and concomitant formation of iron core. Importantly, once formed, these metal-induced cage structures remain intact in low ionic strength solutions which lack ferrous iron. During the metal-induced self-assembly, the AfFtn cage and other ferritins can be potentially loaded with small molecules, nanoparticles or other molecular cargos while avoiding any loss of the protein structure associated with harsh pH treatment required for loading other ferritin cages (*19, 25*). During the iron-mediated self-assembly, it was possible to encapsulate about 400 cisplatin molecule in each AfFtn-AA cage (unpublished data). The encapsulated cargos can be potentially released in a reverse pathway by dissolving the Fe^{3+} cores using reducing agents (e.g. ascorbate). Thus, iron-mediated self-assembly/disassembly of AfFtn cage and hence, potential loading/release of molecular cargo can be elucidated by studying iron oxidation/reduction kinetics of AfFtn (Scheme 1).

Understanding the kinetics and mechanisms of self-assembly/disassembly of protein nanocages is a crucial, but underemphasized and poorly understood area in the development of protein-based drug delivery systems. Some physical and chemical triggers have been successfully used to initiate cargo release from the carrier proteins (*26*). Biological modulation of protein cages may also facilitate in tuning the release of molecular cargos (*27, 28*). Several reports described drug encapsulation and release in ferritin cages by pH variations (*5, 18, 19, 26, 29*). The iron-mediated self-assembly/disassembly property of AfFtn offers a new set of

molecular trigger for formation and dissociation of the protein cage. Study of iron binding kinetics will help to understand iron-mediated self-assembly and simultaneous molecular loading within the ferritin cages while the kinetics of ascorbate-mediated iron release reflect the dissociation and release of cargo from the protein cage.

The crystal structure of the wild-type AfFtn (PDB ID 1SQ3; Figure 1A) shows an atypical open-pore structural conformation (*20*). All other ferritins of known structure form virtually closed cage-like structures with octahedral symmetry. In contrast, the AfFtn subunits self-assemble with tetrahedral symmetry and form a protein cage with four distinct large triangular pores (~45Å) that expose the internal cavity of AfFtn to the outer environment. These open-pores are unique to the *A. fulgidus* ferritin and may offer another potential route for encapsulation of molecular cargos within the AfFtn cages. Potential molecular transport through the pores can be assessed through the variation of physicochemical properties of the protein i.e. by collapsing the large pores. To achieve this, we engineered a closed-pore variant of AfFtn by replacing two positively charged amino acids (K150 and R151) with alanine residues (AfFtn-AA). Subsequent crystallography studies confirmed a massive rearrangement of ferritin subunits; the crystal structure of AfFtn-AA showed a canonical closed protein cage with octahedral symmetry (PDB ID 3KX9; Figure 1B) (*22*). The understanding of iron binding and release kinetics in AfFtn and AfFtn-AA will also help to shed light on the route of molecular transport providing a foundation on which further design and engineering can be used to optimize the molecular release from the intact protein cage. We hypothesize that the iron entry/release profiles of AfFtn-AA will differ from that of the AfFtn if the four large pores are involved in the transport of reactants or products. Preliminary studies showed slower iron release from the closed AfFtn-AA relative to the open AfFtn (*22*). Here we describe the unique iron-mediated self-assembly/disassembly of AfFtn and AfFtn-AA, and comprehensive iron oxidation/reduction kinetics of these proteins. This report also presents the effects of the K150A/R151A mutations on the iron-mediated self-assembly property of AfFtn and the effect of eliminating the large pores on iron entry and release kinetics.

EXPERIMENTAL

All experiments in the following sections including the formation and solubilisation of iron core and, iron binding and release kinetics were performed in aerobic conditions. The results are confirmed by repeating all the experiments at least three times and wherever applicable, the average of three results are reported in the 'Results and Discussion' section.

Production and purification of AfFtn and AfFtn-AA

The mutation was done by PCR based site-directed mutagenesis using a set of complimentary primers containing the altered sequences. K150A/R151A substitution was confirmed by sequencing of the mutated gene cloned in pET-11a vector. For the production of AfFtn or AfFtn-AA proteins, *E. coli* BL21-CodonPlus® (DE3)-RIL competent cells were transformed with construct containing the respective genes. The transformed cells were grown in LB broth media (containing ampicillin and chloramphenicol at 0.1 g/l and 0.05 g/l, respectively) and the overexpression was induced using 1 mM IPTG. Cells were harvested 4 hours post induction and resuspended in 25 mM HEPES buffer, pH 7.5, containing 50 mM NaCl. The cells were disrupted at 15,000 psi pressure using a French press cell disruptor (Thermo Electron Corporation) and the insoluble fraction was removed by ultracentrifugation at 150,000 × *g* at 4°C for 1 hour. AfFtn

and AfFtn-AA were purified by heat treatment at 85°C for 10 minutes and the denatured *E. coli* proteins were removed by centrifugation at 150,000 × *g* at 4°C for 1 hour. The proteins were further purified with ÄKTA-Explorer FPLC system (GE Healthcare) by hydrophobic interaction chromatography using HiPrep 16/10 Phenyl FF (high sub) column. Binding buffer was composed of 25 mM HEPES with 50 mM NaCl and 500 mM ammonium sulfate, pH 7.5, and the same buffer without ammonium sulfate was used for elution of the bound proteins. Purified proteins were concentrated and buffer-exchanged to obtain the final protein preparation of 1 mg/ml protein in 25 mM HEPES, 50 mM NaCl, pH 7.5. Protein concentration was measured by bicinchoninic acid method following the manufacturer's protocol and using bovine serum albumin as standard (BCA protein assay kit, Thermo Scientific). Protein yield was ~20 mg/l culture.

Mineralization and solubilisation of the iron core

$FeSO_4$ solution of 100 mM was prepared in 0.1% HCl and added to 0.1 mg/ml AfFtn-AA solution (in 100 mM HEPES buffer, pH 7.5 with 50 mM NaCl) The mineralization was completed by repeated addition of equal aliquots at a molar ratio of 480 Fe per 24-meric ferritin cage at 10 minutes interval.to reach the desired iron loading. The stepwise addition was important to avoid high local concentrations that led to precipitation. The solution was mixed immediately after each addition. The mixture was incubated for one hour at room temperature and followed by overnight incubation at 4°C. Any suspended particles were removed by centrifuging the mixture at 25,000 × g for 15 minutes and the supernatant was concentrated by membrane filtration using Centricon® (100 kDa MWCO) centrifugal device (Millipore). Any unbound metal was removed by desalting through PD-10 column (GE Healthcare). Hereafter the mineralized AfFtn and AfFtn-AA would be referred as (Fe)AfFtn and (Fe)AfFtn-AA, respectively.

To dissolve the iron core, ascorbate solution was added to mineralized ferritin solution (0.1 mg/ml, containing 480 Fe/24-mer) in the presence of an iron chelating agent (ferrozine) to achieve 1 mM final ascorbate concentration. The mixture was incubated overnight at 37°C prior to size exclusion chromatography analysis.

Transmission electron microscopy

(Fe)AfFtn or (Fe)AfFtn-AA solution (0.1mg/ml in 10 mM HEPES buffer, pH 7.5) was applied directly onto carbon coated copper grids and allowed to adhere for 2 minutes. Excess solution was removed by wicking with filter paper and grids were allowed to air dry. The samples were stained with 1% uranyl acetate for another 2 minutes and air dried after wicking the excess uranyl acetate solution. Specimens were examined with 30,000x magnification in a JEOL JEM-1400 transmission electron microscope at an accelerating voltage of 100 kV.

Size exclusion chromatography

Iron-mediated self-assembly and ascorbate-mediated disassembly were studied by size exclusion chromatography (SEC) using Superdex 200 10/300 GL column (GE Healthcare). Molecular sizes of AfFtn or AfFtn-AA were determined at different conditions by comparing their elution volume with that of standard proteins. Molecular weights of AfFtn/AfFtn-AA were determined by analyzing 500 µl of each species before mineralization, after mineralization, and after reduction of the metal core. Composition of the mobile phase was 25 mM HEPES with 50 mM

sodium chloride, pH 7.5. All SEC experiments were performed using ÄKTA-Explorer FPLC system (GE Healthcare).

Iron binding kinetics

Iron binding kinetics of AfFtn and AfFtn-AA were studied at different Fe^{2+} concentrations (in 100 mM HEPES buffer, pH 7.5 with 50 mM NaCl). Dilute protein solutions (0.1 mg/ml) were used to avoid fast autoxidation at higher Fe^{2+} concentrations. The reaction was started by addition of 10 µl freshly prepared $FeSO_4$ stock solution in 1ml of 0.1 mg/ml AfFtn solution (pre-incubated at the specified temperature within temperature-controlled spectrophotometer), and mixed immediately by pipetting within one second. The stock concentration was adjusted to achieve the desired iron concentration in the final reaction mixture. Iron binding was monitored in terms of Fe^{2+} oxidation, measured colorimetrically, following the increase of absorbance at 315 nm measured every 2 seconds. Fe^{3+} was quantified using molar absorption coefficient ε_{315} = 2,200 $M^{-1}cm^{-1}$ (*30*).

Iron release kinetics

Reductive iron release profiles of (Fe)AfFtn and (Fe)AfFtn-AA were studied using varying concentrations of ascorbate (reducing agent) at 70°C. The effect of temperature on the rate of Fe^{2+} release was also studied with 10 mM ascorbate and the activation energy (E_a) for iron release was calculated from the Arrhenius plot. (Fe)AfFtn and (Fe)AfFtn-AA (0.1 mg/ml containing 4800 Fe/24-mer) were incubated at various temperatures with 1 mM ferrozine in a temperature-controlled spectrophotometer. The reaction was started by addition of ascorbate and iron release was measured by monitoring the formation of Fe^{2+}-ferrozine complex at 562 nm. The iron release rate was determined using a molar absorption coefficient of ε_{562} = 27.9 mM^{-1} cm^{-1} for the iron ferrozine complex.

RESULTS AND DISCUSSION

Iron-mediated self-assembly and ascorbate-mediated dissociation of the protein cage

The effect of K150A/R151A mutations on the iron-mediated self-assembly and ascorbate-mediated disassembly of the AfFtn was studied by SEC, which separates different oligomers by their molecular size. Identical peak-shifts confirmed that AfFtn-AA retains the iron-mediated self-assembly property of AfFtn (Figure 2A). The oligomeric state of each species was estimated from their molecular size. In the absence of iron, both proteins exist mostly as dimer (~40 kDa). Upon mineralization (with 480 Fe/24-mer), the dimers self-assemble to form 24-meric (~490 kDa) cage-like structures. The stabilization of 24-mer via mineralization is stable in nature i.e. the 24-meric structure remains assembled when the mineralized protein cage is exchanged into the same buffer without any iron. The 24-meric protein cage disassembles only after complete dissolution of the iron core by reduction with excess reducing agent in the presence of the iron chelating agent, ferrozine (Figure 2B). The chromatograms suggest nearly identical disassembly properties of AfFtn and AfFtn-AA. Electron microscopy of mineralized samples further confirms the self-assembled cage-like structure of the AfFtn and AfFtn-AA (Figure 3). We propose that for iron-mediated self-assembly, the mineral core itself interacts with the protein shell in such a way that enhances inter-subunit interactions and stabilizes the 24-meric structure. Addition of 20 Fe^{2+} ion per (AfFtn or AfFtn-AA) subunit results in complete self-assembly, which suggests that initial iron binding to the ferroxidase sites enhances inter-dimer interaction that leads to self-assembly of the protein cage. Reduction of the entire iron content required several minutes and

the iron release rate gradually decreased until the end of the reaction (*22*). These observations indicate that the cage structure was maintained until the last few Fe^{3+} were bound to the cage; otherwise dissociation of the protein cage would cause sudden release of all iron and their instant reduction.

The amino acid replacements on AfFtn-AA causes a massive rearrangement of the dimers in quaternary structure and results in a switch from tetrahedral to octahedral symmetry as shown in the crystal structure (*22*). The self-assembly of the ferritin subunits is characterized by two-, three-, and four-fold symmetry axes. The interfaces between subunits are stabilized by hydrophobic and hydrophilic interactions, hydrogen bonding and van der Waals forces. Several hydrophobic contacts were identified at subunit interfaces of the AfFtn and AfFtn-AA structures. AfFtn and its mutant showed a NaCl-mediated self-assembly in a dose-dependent manner, which suggests that hydrophobic interaction is the key force of the self-assembly of AfFtn subunits (*20, 22, 25*). In the presence of 150 mM NaCl, about 80% dimeric subunits of these ferritins reversibly self-assemble into cages, which could be potentially used for developing a drug delivery strategy. Replacement of large hydrophilic Lys150 and Arg151 with alanine residues removes steric clashes and enhances hydrophobic interactions that facilitate self-assembly of AfFtn-AA. However, the exact mechanism of iron-mediated and NaCl-mediated self-assembly of AfFtn/AfFtn-AA remains to be precisely established.

Almost all reported ferritins have a constitutive 24-meric cage-like structure that is used for storage of excess physiological iron and, iron-mediated self-assembly/disassembly has not been reported for these protein cages. However, a new member of the ferritin super-family, and some closely related proteins, have been reported to be dimeric in normal buffers and showed self-assembly characteristics very similar to AfFtn and its mutant (*31, 32*). An archaeoferritin (classified as a member of an uncharacterized branch of the ferritin-like super-family) from the marine archaea *Pyrococcus furiosus*, a very close relative of *A. fulgidus*, was reported to show iron-mediated self-assembly/disassembly property similar to the AfFtn and AfFtn-AA (*31*). *P. furiosus* ferritin showed monomeric structure in the absence of iron and self-assembled into 24-mer in the presence of 30 Fe^{2+} per monomer; it was also possible to dissociate the 24-mer by chemical reduction of the iron core followed by chelation. A ferritin-like Dps protein (DNA-binding protein during starvation) from the extremophilic bacterium *Deinococcus radiodurans* was reported to show DNA-binding ability even at dimeric conformation and form dodecameric structure at high salt concentration (*32*). In combination with the current knowledge of *A. fulgidus* ferritin, further understanding of structural features and association/dissociation properties of these members of ferritin super-family may elucidate the self-assembly/disassembly mechanism of AfFtn and similar ferritin-like molecules. This knowledge would be extremely useful in exploiting these protein cages for drug delivery and nanotechnology applications.

Iron binding kinetics

Our previous study on the iron binding kinetics of AfFtn and AfFtn-AA suggested multiphasic nature of the iron binding reaction (*22*). Here, we report the iron binding kinetics at two different temperatures and the initial binding rates were measured at different Fe^{2+} concentrations. Iron binding kinetics changed with temperature and faster iron binding was observed at higher temperature (Figure 4). Also, the iron binding rate increased proportionally with Fe^{2+} concentrations. The ferroxidase activity in AfFtn and AfFtn-AA was inhibited in the presence of Zn^{2+} ion. The Lineweaver-Burk plots demonstrate the competitive nature of the Zn^{2+}-mediated inhibition of the ferroxidase activity (Figure 5). Previous studies suggest that the nature of this

inhibition is dependent on Zn^{2+} concentration (*33*). At very low concentration (Zn/ferritin ratio ≤ 2) non-competitive inhibition was observed while competitive inhibition occurred at higher proportions of Zn^{2+}. In the present study, the observation of competitive inhibition at much higher Zn/ferritin ratio agrees with the published findings. Competitive inhibition of Fe^{2+} oxidation in the presence of Zn^{2+} indicates that Zn^{2+} binds at the ferroxidase center. Metal binding at the ferroxidase center is a well-known phenomenon in other ferritins and Zn^{2+} binding is also observed in the crystal structure of AfFtn (*20*).

Like iron-mediated self-assembly, the iron binding kinetics are almost identical for AfFtn and AfFtn-AA (Figure 4). The overall iron binding was completed by a multiphasic reaction. Immediate oxidation of iron at the ferroxidase centers (FCs) is observed in an initial fast reaction phase, followed by a slower oxidation phase at the nucleation site. The latter phase requires transport of Fe^{2+} ion into the cavity through some pores/channels on the protein surface. The initial rate of iron oxidation was not be expected to differ between the open and closed form (i.e. AfFtn to AfFtn-AA) because the FCs, which are located in the 4-helix bundle of each subunit, remain equally accessible. The current theory is that the initial iron binding occurs at the FCs where Fe^{2+} oxidizes to Fe^{3+} and the Fe^{3+} product is transported to the nucleation site (*14, 34, 35*). Once nucleation occurs, Fe^{2+} can enter via the 3-fold channels (or the large pores for the AfFtn) and spontaneously bind and mineralize at the nucleus without ferroxidase activity. Approximately equal Fe^{2+} oxidation rates were expected in AfFtn and AfFtn-AA at the early stage (FC-based oxidation). However, if entry of Fe^{2+} through the closed shell was rate limiting, a faster oxidation rate for the open AfFtn should be observed at the later, ferroxidase independent phase. The identical Fe^{2+} oxidation kinetics throughout the reaction suggests that the large pore of AfFtn may not play any role in the transport of Fe^{2+} to the nucleation site.

Fe^{2+} oxidation within ferritin is distinct from typical enzymatic reactions because the product is deposited within the enzyme itself instead of being released into the reaction mixture. Once the core is fully loaded no more oxidation is observed – such inactivation is not commonly observed in other enzymatic reactions. It has been established that Fe^{2+} oxidation within ferritin is a very fast process that may be completed in the order of milliseconds to minutes depending on iron concentration, physical condition, and the exact catalytic activity of the protein while Fe^{3+} ion transport and core formation take minutes to hours (*34, 36, 37*). A previous study showed that the rate of Fe^{2+} oxidation was relatively slow when the ferritin cage is partially loaded with iron (*38*). The authors suggest that the presence of high Fe^{3+} concentration at the nucleation site may inhibit ferroxidase activity. However, as the nucleation site is distinct from the catalytic site, the core formation may not affect the ferroxidase activity. Rather the entire process may be inhibited in the subsequent steps of the multiphasic reaction.

Iron release kinetics

The rate of reductive iron release from both ferritins is highly dependent on temperature and concentration of the reducing agent (Figure 6 and Figure 7). In all conditions, the initial iron release during ascorbate-mediated Fe^{3+} reduction is faster for the open-pore AfFtn than the closed mutant AfFtn-AA. Similar results were observed with two other reducing agents, dihydroxyfumaric acid and NADH (data not shown); the experiments were done following the published methods (*36, 39, 40*).

At 70°C, the initial rate of Fe^{2+} release from AfFtn-AA is 2/3 to 1/2 of that from AfFtn at any ascorbate concentration (Figure 6). The initial iron release rate sharply increases as the ascorbate concentration increases to 2 mM and reaches a maximum above 5 mM ascorbate

concentration. Iron release is temperature sensitive; as the temperature increases from 20°C to 76°C, the initial iron release rate increases more than four times for both AfFtn and AfFtn-AA and has not reached the maximum at the highest temperature of the experiment (Figure 7). The activation energies for iron release for AfFtn and AfFtn-AA calculated from the Arrhenius plot are 44.4 kJ mole^{-1} and 46.3 kJ mole^{-1}, respectively. These values are comparable to previously reported values of activation energy of iron release from *Azotobacter vinelandii* ferritin (60 kJ mole^{-1}) and horse spleen ferritin (10.2 kJ mole^{-1}) (*41, 42*) as well as other thermophilic archaeal enzymes (*43, 44*).

The slower iron release rate in the closed variant suggests that the large pores of AfFtn play some role in the reductive iron release mechanism. The K150A/R151A mutation results in a switch in symmetry from an open tetrahedral cage to a closed octahedral structure. The closed assembly diminishes the accessibility of ascorbate reducing equivalents to the AfFtn-AA core and decreases the ascorbate mediated iron release rate. We hypothesize that the transport of reducing agent or the reduced Fe^{2+} ion is slower in AfFtn-AA because the narrow 3- or 4-fold channels are used for their transport instead of the large pores of AfFtn.

Despite *in vitro* studies of the reductive iron release kinetics for ferritins from several species the mechanism of iron release remains unclear. The ferritin iron core was reported to be heterogeneous and therefore the mechanism of iron mobility may vary depending on the nature of the environment in which the cage is formed, the initial iron loading, and the extent of reaction (*45-47*). The mechanism seems to be complex and consists of multiple steps. A typical *in vitro* iron release reaction can be described as (1) entry of reducing equivalent into the protein cage, (2) reduction of the Fe^{3+} to Fe^{2+}, (3) exit of Fe^{2+} from the protein cage, and (4) chelation of the Fe^{2+} with chelating agents (*42, 48*). Two reduction models have been proposed: (1) the reducing agent physically enters the ferritin and (2) only electrons are transferred from the external reductants to the protein core (*48-50*). The latter model is generally accepted if the molecular size of the reducing agent is larger than the channel diameter. One report suggests flexible ferritin channels which open to allow passage of larger reducing molecules (*50*). Another model proposes that the chelating agents need to enter the ferritin cage to remove the reduced Fe^{2+} ions and later the chelates exit the ferritin cage (*51*). The initial iron mobilization rate was reported to be dependent on the concentration of reducing agent but not on the concentration of the chelating agent suggesting that chelation is not involved in any rate-limiting step (*39*).

In general, mineralization and demineralization of ferritin are complex processes associated with transport, oxidation or reduction of metal ions. Fe^{3+} core formation requires Fe^{2+} to be transported from the outer environments to the catalytic site and from the catalytic site to the nucleation/mineralization site. In contrast, iron release is associated with iron transport from the mineralization site to the outer environment. Oxidation and reduction is also dependent on transport of oxidizing and reducing equivalents, electrons, and protons. The movements of protons, electrons, ions, and molecules in and out of ferritin cages have been widely studied but the transport mechanisms remain unclear. Several pores and ion channels within the cage structure are likely to be used for this purpose. Mutational analyses of these pores and channels have been performed to understand their roles in the transport mechanisms. AfFtn has a novel tetrahedral structure with four large triangular pores, which present a potential pathway for the transport of ions and small molecules. Conversion to a closed octahedral shell shows that the pores have no effect on iron entry kinetics. In contrast, the reductive iron release rate of the open AfFtn is faster than the closed AfFtn-AA, suggesting that the large pores play some roles in iron release. Previous reports discussed the iron entry and release pathways in various ferritin

molecules and alteration of channels or pores was shown to affect iron entry and release kinetics (*36*, *40*, *52*). Localized unfolding at the 3-fold axis has been reported upon a single point mutation of frog ferritin, which decreases entry rate and increases initial iron release rate by several fold (*52*). In another study, increased iron release rates were observed in several single point mutations near 3-fold channels but none of the mutations caused significant change in the rate of Fe^{2+} oxidation (*36*). Liu et al. showed that the presence of chaotropes at low concentrations significantly increased the initial iron release rate from the recombinant frog ferritin but observed only a minor inhibition of the Fe^{2+} ion entry even at very high chaotrope concentrations (*40*). All these observations suggest that there are specific and independent routes for transport of different ions and molecules essential for iron entry and release. Mutational change of one pore or channel may affect the transport of selective ions/molecules and alter the associated reaction (binding or release) without affecting the other. Studies of iron entry and release kinetics in a number of natural and recombinant ferritins suggest that each process is likely to operate using more than one pathway (*14*, *38*, *53-55*). At least three alternative reactions have been observed for conversion of Fe^{2+} to FeOOH core; the proportion of each reaction in the overall core formation procedure depends on the reaction environment, Fe/ferritin ratio and Fe/O_2 ratio (*14*, *15*). The overall core formation procedure was multiphasic and different types of progression curves were noticed for the wild-type ferritin and different mutants (*14*). Iron deposition is dependent on Fe^{2+} ion oxidation that is faster at higher temperature, higher pH, or in the presence of oxidizing agent (H_2O_2) (*55*). The reaction was >20 time faster in the presence of H_2O_2 than in O_2 alone. The rate of ferroxidase center catalyzed oxidation was reported to be faster at higher Fe^{2+} concentration (*38*). The results of the present experiments also show a faster initial reaction rate at higher Fe^{2+} concentration.

CONCLUSION

Archaeoglobus fulgidus ferritin (AfFtn) and its mutant (AfFtn-AA) exhibit unique self-assembly/disassembly property that can be exploited for their applications as a molecular carrier. The dimeric AfFtn or AfFtn-AA self-assembles into stable cage-like structure following addition of Fe^{2+} ion and subsequent Fe^{3+} core synthesis. The protein cages can then be dissociated by reducing the Fe^{3+} core in the presence of excess ascorbate (reducing agent). The iron-mediated self-assembly can potentially encapsulate small molecules or nanoparticles present within the medium and the encapsulated cargo can be released by reductive dissociation of the protein cage. The identical iron entry kinetics of the open-pore AfFtn and closed AfFtn-AA cages suggests that the iron transport channels of AfFtn remains unchanged by this mutation. Slower iron release kinetics has been observed in AfFtn-AA and the current study shows reduced iron release rate in the closed mutant over a range of temperature and ascorbate concentration, which support the involvement of the large pores in the reductive iron release process. Competitive inhibition of iron binding in the presence of Zn^{2+} ion evidenced the AfFtn affinity to other metals.

FUNDING

This work was funded by Singapore Ministry of Education Academic Research Fund Tier I (RG33/07).

References

1. Dalmau, M., Lim, S., Chen, H. C., Ruiz, C., and Wang, S.-W. (2008) Thermostability and molecular encapsulation within an engineered caged protein scaffold, *Biotechnology and Bioengineering 101*, 654-664.
2. Georgens, C., Weyermann, J., and Zimmer, A. (2005) Recombinant virus like particles as drug delivery system, *Current Pharmaceutical Biotechnology 6*, 49-55.
3. Kasyutich, O., Ilari, A., Fiorillo, A., Tatchev, D., Hoell, A., and Ceci, P. (2010) Silver ion incorporation and nanoparticle formation inside the cavity of *Pyrococcus furiosus* ferritin: Structural and size-distribution analyses, *Journal of the American Chemical Society 132*, 3621-3627.
4. MaHam, A., Tang, Z., Wu, H., Wang, J., and Lin, Y. (2009) Protein-based nanomedicine platforms for drug delivery, *Small 5*, 1706-1721.
5. MaHam, A., Wu, H., Wang, J., Kang, X., Zhang, Y., and Lin, Y. (2011) Apoferritin-based nanomedicine platform for drug delivery: equilibrium binding study of daunomycin with DNA, *Journal of Materials Chemistry 21*, 8700-8708.
6. Sun, C., Yang, H., Yuan, Y., Tian, X., Wang, L., Guo, Y., Xu, L., Lei, J., Gao, N., Anderson, G. J., Liang, X.-J., Chen, C., Zhao, Y., and Nie, G. (2011) Controlling Assembly of Paired Gold Clusters within Apoferritin Nanoreactor for in Vivo Kidney Targeting and Biomedical Imaging, *Journal of the American Chemical Society 133*, 8617-8624.
7. Uchida, M., Klem, M. T., Allen, M., Suci, P., Flenniken, M., Gillitzer, E., Varpness, Z., Liepold, L. O., Young, M., and Douglas, T. (2007) Biological Containers: Protein Cages as Multifunctional Nanoplatforms, *Advanced Materials 19*, 1025-1042.
8. Yan, C., Lian, X., Dai, Y., Wang, X., Qu, P., White, A., Qin, Y., and Du, H. (2007) Gene delivery by the hSP-B promoter to lung alveolar type II epithelial cells in LAL-knockout mice through bone marrow mesenchymal stem cells, *Gene Ther 14*, 1461-1470.
9. Zheng, B., Yamashita, I., Uenuma, M., Iwahori, K., Kobayashi, M., and Uraoka, Y. (2010) Site-directed delivery of ferritin-encapsulated gold nanoparticles, *Nanotechnology 21*, 045305.
10. Lin, X., Xie, J., Zhu, L., Lee, S., Niu, G., Ma, Y., Kim, K., and Chen, X. (2011) Hybrid Ferritin Nanoparticles as Activatable Probes for Tumor Imaging, *Angewandte Chemie International Edition 50*, 1569-1572.
11. Mohie-Eldin, M. E. Y., Frankel, R. B., Gunther, L., and Papaefthymiou, G. C. (1995) The anomalous Mössbauer fraction of ferritin and polysaccharide iron complex (PIC), *Hyperfine Interact 96*, 111-138.
12. Marinova, M., and Vladimirova, L. (2010) Atomic Absorption Assessment of Mineral Iron Quantity in Ferritin, *Spectroscopy Letters 43*, 192-195.
13. Chasteen, N. D., and Harrison, P. M. (1999) Mineralization in Ferritin: An Efficient Means of Iron Storage, *Journal of Structural Biology 126*, 182-194.
14. Zhao, G., Bou-Abdallah, F., Arosio, P., Levi, S., Janus-Chandler, C., and Chasteen, N. D. (2003) Multiple pathways for mineral core formation in mammalian apoferritin. The role of hydrogen peroxide, *Biochemistry 42*, 3142-3150.
15. Yang, X., Chen-Barrett, Y., Arosio, P., and Chasteen, N. D. (1998) Reaction paths of iron oxidation and hydrolysis in horse spleen and recombinant human ferritins, *Biochemistry 37*, 9743-9750.

16. Douglas, T., and Ripoll, D. R. (1998) Calculated electrostatic gradients in recombinant human H-chain ferritin, *Protein Science 7*, 1083-1091.
17. Takahashi, T., and Kuyucak, S. (2003) Functional properties of threefold and fourfold channels in ferritin deduced from electrostatic calculations, *Biophysical journal 84*, 2256-2263.
18. Aime, S., Frullano, L., and Geninatti Crich, S. (2002) Compartmentalization of a gadolinium complex in the apoferritin cavity: A route to obtain high relaxivity contrast agents for magnetic resonance Imaging, *Angewandte Chemie 114*, 1059-1061.
19. Simsek, E., and Akif Kilic, M. (2005) Magic ferritin: A novel chemotherapeutic encapsulation bullet, *Journal of Magnetism and Magnetic Materials 293*, 509-513.
20. Johnson, E., Cascio, D., Sawaya, M. R., Gingery, M., and Schröder, I. (2005) Crystal structures of a tetrahedral open pore ferritin from the hyperthermophilic archaeon *Archaeoglobus fulgidus*, *Structure 13*, 637-648.
21. Sana, B., Calista, M., and Lim, S. (2012) Protein cage assisted metal-protein nanocomposite synthesis: Optimization of loading conditions, *AIP Conference Proceedings 1502*, 82-96.
22. Sana, B., Johnson, E., Le Magueres, P., Criswell, A., Cascio, D., and Lim, S. (2013) The role of non-conserved residues of Archaeoglobus fulgidus ferritin on its unique structure and biophysical properties, *Journal of Biological Chemistry 288*, 32663-32672.
23. Sana, B., Johnson, E., Sheah, K., Poh, C. L., and Lim, S. (2010) Iron-based ferritin nanocore as a contrast agent, *Biointerphases 5*, 48-52.
24. Sana, B., Poh, C. L., and Lim, S. (2012) A manganese-ferritin nanocomposite as an ultrasensitive T_2 contrast agent, *Chemical Communications 48*, 862-864.
25. Swift, J., Butts, C. A., Cheung-Lau, J., Yerubandi, V., and Dmochowski, I. J. (2009) Efficient self-assembly of *Archaeoglobus fulgidus* ferritin around metallic cores, *Langmuir 25*, 5219-5225.
26. Flenniken, M. L., Liepold, L. O., Crowley, B. E., Willits, D. A., Young, M. J., and Douglas, T. (2005) Selective attachment and release of a chemotherapeutic agent from the interior of a protein cage architecture, *Chemical Communications*, 447-449.
27. Peng, T., and Lim, S. (2011) Trimer-Based Design of pH-Responsive Protein Cage Results in Soluble Disassembled Structures, *Biomacromolecules 12*, 3131-3138.
28. Zhang, Y., Fu, J., Chee, S. Y., Ang, E. X. W., and Orner, B. P. (2011) Rational disruption of the oligomerization of the mini-ferritin E. coli DPS through protein-protein interface mutation, *Protein Science 20*, 1907-1917.
29. Webb, B., Frame, J., Zhao, Z., Lee, M. L., and Watt, G. D. (1994) Molecular Entrapment of Small Molecules within the Interior of Horse Spleen Ferritin, *Archives of Biochemistry and Biophysics 309*, 178-183.
30. Bonomi, F., Kurtz Jr, D. M., and Cui, X. (1996) Ferroxidase activity of recombinant *Desulfovibrio vulgaris* rubrerythrin, *Journal of Biological Inorganic Chemistry 1*, 67-72.
31. Ebrahimi, K., Hagedoorn, P.-L., van der Weel, L., Verhaert, P. E. M., and Hagen, W. (2012) A novel mechanism of iron-core formation by Pyrococcus furiosus archaeoferritin, a member of an uncharacterized branch of the ferritin-like superfamily, *J Biol Inorg Chem 17*, 975-985.
32. Grove, A., and Wilkinson, S. P. (2005) Differential DNA Binding and Protection by Dimeric and Dodecameric forms of the Ferritin Homolog Dps from Deinococcus radiodurans, *Journal of Molecular Biology 347*, 495-508.

33. Sun, S., and Chasteen, N. D. (1992) Ferroxidase kinetics of horse spleen apoferritin, *Journal of Biological Chemistry 267*, 25160-25166.
34. Bou-Abdallah, F. (2010) The iron redox and hydrolysis chemistry of the ferritins, *Biochimica et Biophysica Acta (BBA) - General Subjects 1800*, 719-731.
35. Santambrogio, P., Levi, S., Cozzi, A., Corsi, B., and Arosio, P. (1996) Evidence that the specificity of iron incorporation into homopolymers of human ferritin L- and H-chains is conferred by the nucleation and ferroxidase centres, *Biochemical Journal 314*, 139-144.
36. Jin, W., Takagi, H., Pancorbo, B., and Theil, E. C. (2001) "Opening" the ferritin pore for iron release by mutation of conserved amino acids at interhelix and loop sites, *Biochemistry 40*, 7525-7532.
37. Tosha, T., Behera, R. K., Ng, H. L., Bhattasali, O., Alber, T., and Theil, E. C. (2012) Ferritin protein nanocage ion channels: Gating by N-terminal extensions, *Journal of Biological Chemistry 287*, 13016-13025.
38. Bou-Abdallah, F., Zhao, G., Mayne, H. R., Arosio, P., and Chasteen, N. D. (2005) Origin of the unusual kinetics of iron deposition in human H-chain ferritin, *Journal of the American Chemical Society 127*, 3885-3893.
39. Boyer, R. F., Grabill, T. W., and Petrovich, R. M. (1988) Reductive release of ferritin iron: A kinetic assay, *Analytical Biochemistry 174*, 17-22.
40. Liu, X., Jin, W., and Theil, E. C. (2003) Opening protein pores with chaotropes enhances Fe reduction and chelation of Fe from the ferritin biomineral, *Proceedings of the National Academy of Sciences 100*, 3653-3658.
41. Macur, R. E., Olsen, R. A., and Inskeep, W. P. (1991) Photochemical mobilization of ferritin iron, *Plant and Soil 130*, 69-74.
42. Richards, T. D., Pitts, K. R., and Watt, G. D. (1996) A kinetic study of iron release from *Azotobacter vinelandii* bacterial ferritin, *Journal of Inorganic Biochemistry 61*, 1-13.
43. Lim, S., Springstead, J. R., Yu, M., Bartkowski, W., Schroder, I., and Monbouquette, H. G. (2009) Characterization of a key trifunctional enzyme for aromatic amino acid biosynthesis in Archaeoglobus fulgidus, *Extremophiles 13*, 191-198.
44. Lim, S., Schroder, I., and Monbouquette, H. G. (2004) A thermostable shikimate 5-dehydrogenase from the archaeon Archaeoglobus fulgidus, *FEMS Microbiol Lett 238*, 101-106.
45. Cowley, J. M., Janney, D. E., Gerkin, R. C., and Buseck, P. R. (2000) The structure of ferritin cores determined by electron nanodiffraction, *Journal of Structural Biology 131*, 210-216.
46. Gálvez, N., Fernández, B. n., Sánchez, P. n., Cuesta, R., Ceolín, M., Clemente-León, M., Trasobares, S., López-Haro, M., Calvino, J. J., Stéphan, O., and Domínguez-Vera, J. M. (2008) Comparative structural and chemical studies of ferritin cores with gradual removal of their iron contents, *Journal of the American Chemical Society 130*, 8062-8068.
47. Quintana, C., Cowley, J. M., and Marhic, C. (2004) Electron nanodiffraction and high-resolution electron microscopy studies of the structure and composition of physiological and pathological ferritin, *Journal of Structural Biology 147*, 166-178.
48. Ji, X., Huang, L., Lin, Q., and Huang, H. (2012) Characteristics and kinetics of iron releasefrom the ferritin under the EGCG reduction, *Biological Trace Element Research 146*, 134-140.

49. Watt, G. D., Jacobs, D., and Frankel, R. B. (1988) Redox reactivity of bacterial and mammalian ferritin: is reductant entry into the ferritin interior a necessary step for iron release?, *Proceedings of the National Academy of Sciences 85*, 7457-7461.
50. Yang, D., and Nagayama, K. (1995) Permeation of small molecules into the cavity of ferritin as revealed by proton nuclear magnetic resonance relaxation, *Biochemical Journal 307*, 253-256.
51. Sánchez, P., Gálvez, N., Colacio, E., Mirñones, E., and Domínguez-Vera, J. M. (2005) Catechol releases iron(III) from ferritin by direct chelation without iron(II) production, *Dalton Transactions*, 811-813.
52. Takagi, H., Shi, D., Ha, Y., Allewell, N. M., and Theil, E. C. (1998) Localized unfolding at the junction of three ferritin subunits, *Journal of Biological Chemistry 273*, 18685-18688.
53. Brown, D. A., Herlihy, K. M., and O'Shea, S. K. (1999) Kinetics of iron(III) chelation from polynuclear oxo-hydroxy aggregates by hydroxamic acids: understanding ferritin iron(III) sequestration, *Inorganic Chemistry 38*, 5198-5202.
54. Kong, B., Huang, H.-Q., Lin, Q.-M., Kim, W.-S., Cai, Z., Cao, T.-M., Miao, H., and Luo, D.-M. (2003) Purification, electrophoretic behavior, and kinetics of iron release of liver ferritin of *Dasyatis akajei*, *Journal of Protein Chemistry 22*, 61-70.
55. Lowery Jr, T. J., Bunker, J., Zhang, B., Costen, R., and Watt, G. D. (2004) Kinetic studies of iron deposition in horse spleen ferritin using H_2O_2 and O_2 as oxidants, *Biophysical Chemistry 111*, 173-181.

FIGURE LEGENDS

Scheme 1. Schematic presentation of a proposed iron-mediated self-assembly and ascorbate-mediated disassembly of AfFtn. (1) Fe^{3+} core formation and self-assembly by Fe^{2+} (shown as brown droplets) addition, (2) reduction of Fe^{3+} core by ascorbate (shown as blue droplets) and (3) ascorbate-mediated disassembly of AfFtn cage.

Figure 1. Structures of the open-pore *A. fulgidus* ferritin AfFtn (A) and the closed-pore AfFtn-AA (B) showing the locations of amino acid residues 150 (red) and 151 (blue).

Figure 2. Elution volume of AfFtn (black) and AfFtn-AA (red) as determined by SEC. (A) Solid and dashed lines indicate holo- and apo-ferritin, respectively. (B) Solid and dashed lines indicate mineralized samples with the iron core and mineralized samples after reduction of iron core, respectively. The mineralized samples contain 480 Fe/24-mer.

Figure 3. Electron micrographs of iron-loaded ferritin (A) (Fe480)AfFtn and (B) (Fe480)AfFtn-AA negative stained with uranyl acetate.

Figure 4. Iron entry in AfFtn (black), AfFtn-AA (red) at 37 °C (solid) and 20 °C (dashed).

Figure 5. Lineweaver-Burk plot for ferroxidase activity and inhibition by 25 μM and 100 μM Zn. Solid (red) lines are for AfFtn-AA with/without inhibitor and the dashed (black) line indicates AfFtn without inhibition.

Figure 6. Initial iron release rate of AfFtn (black, solid) and AfFtn-AA (red, dashed) at different ascorbate concentrations at 70 °C and pH 7.5.

Figure 7. Initial iron release rate of AfFtn (black, solid) and AfFtn-AA (red, dashed) at different temperatures. Arrhenius plot generated for iron release from (Fe)AfFtn (black, solid) and (Fe)AfFtn-AA (red, dashed) over the temperature range 20-50°C (inset).

Scheme 1.

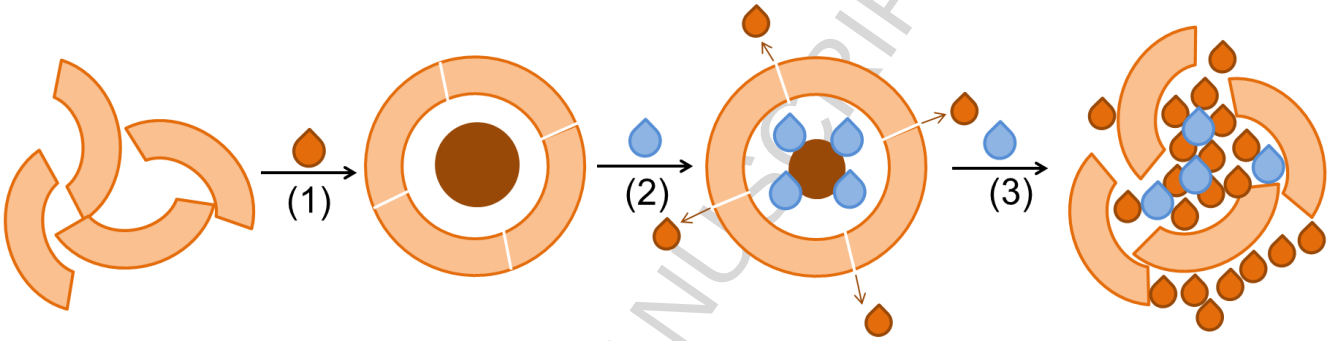

Figure 1.

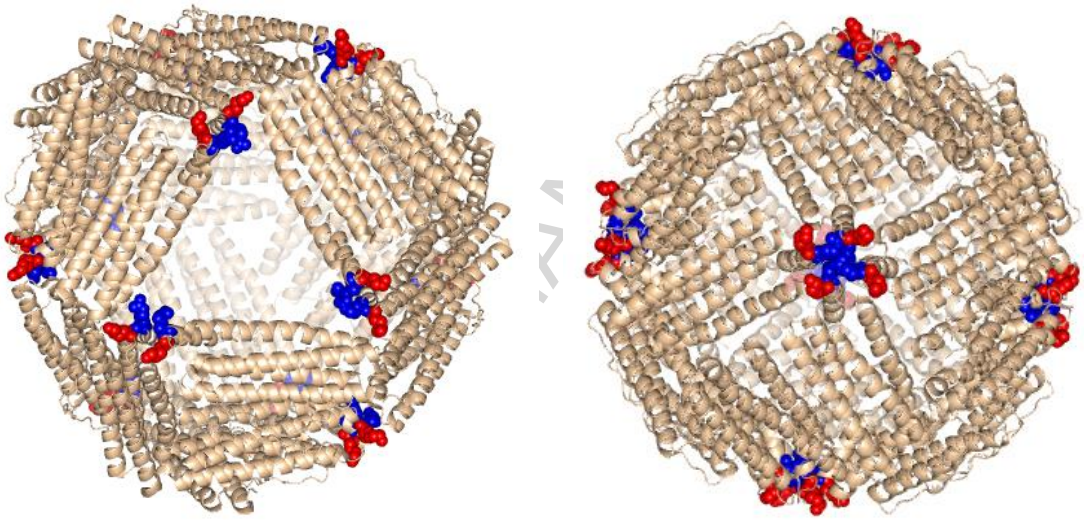

(A) **(B)**

Figure 2.

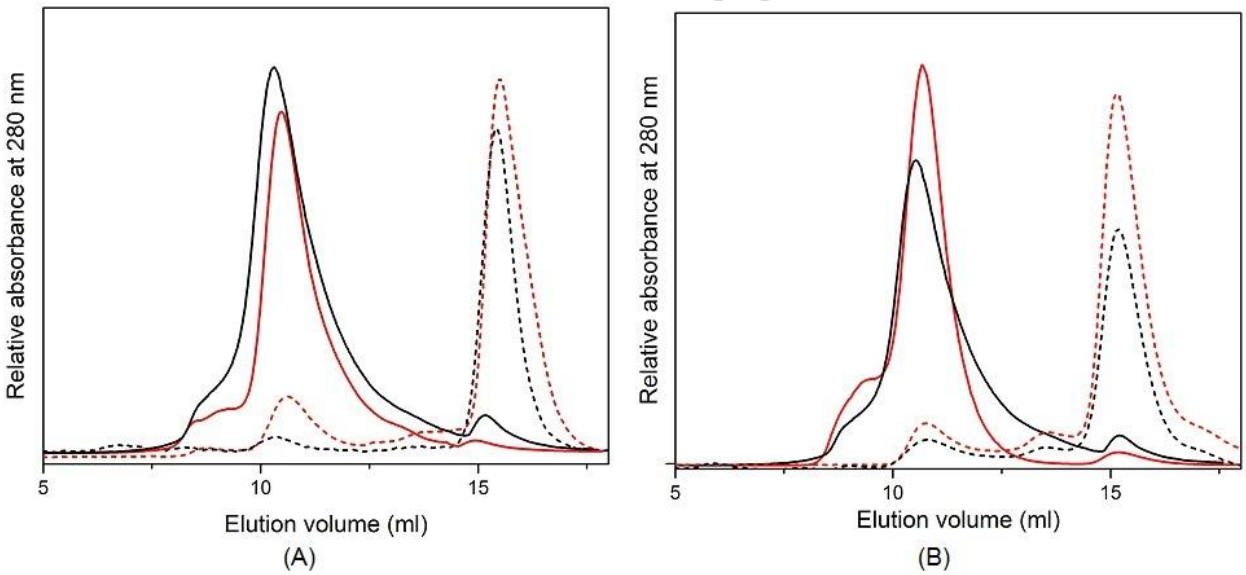

Figure 3.

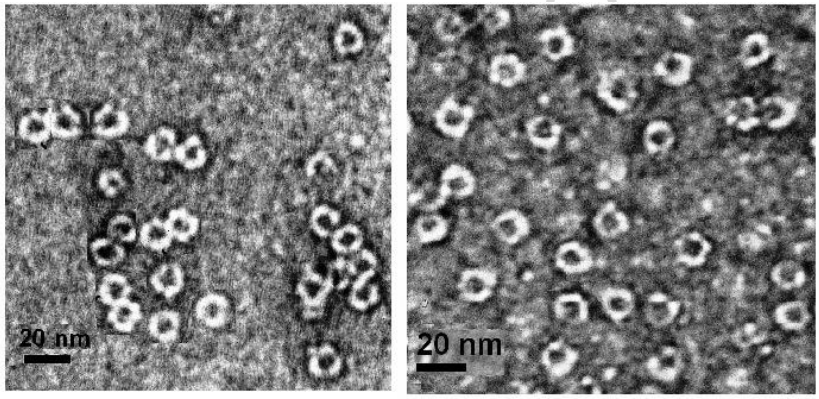

(A) **(B)**

Figure 4.

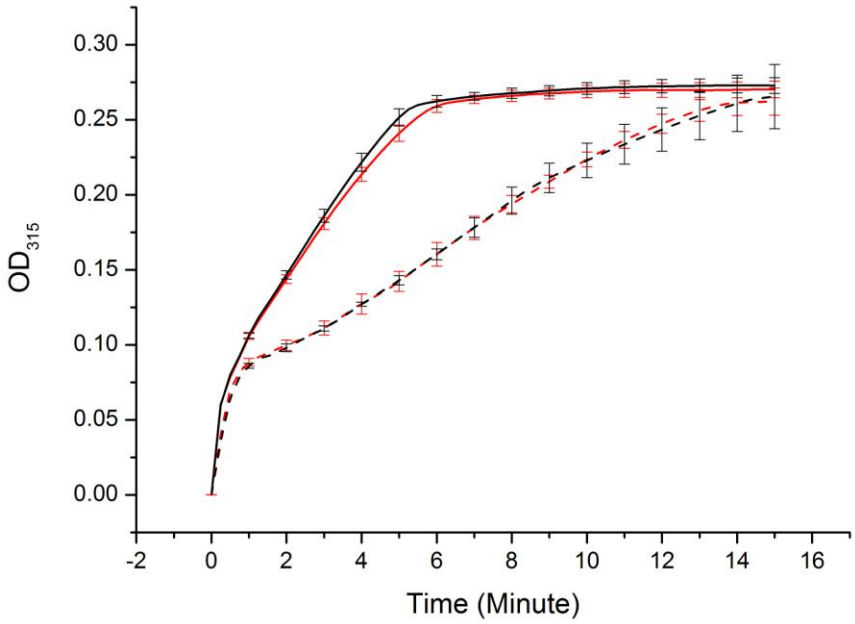

Figure 5.

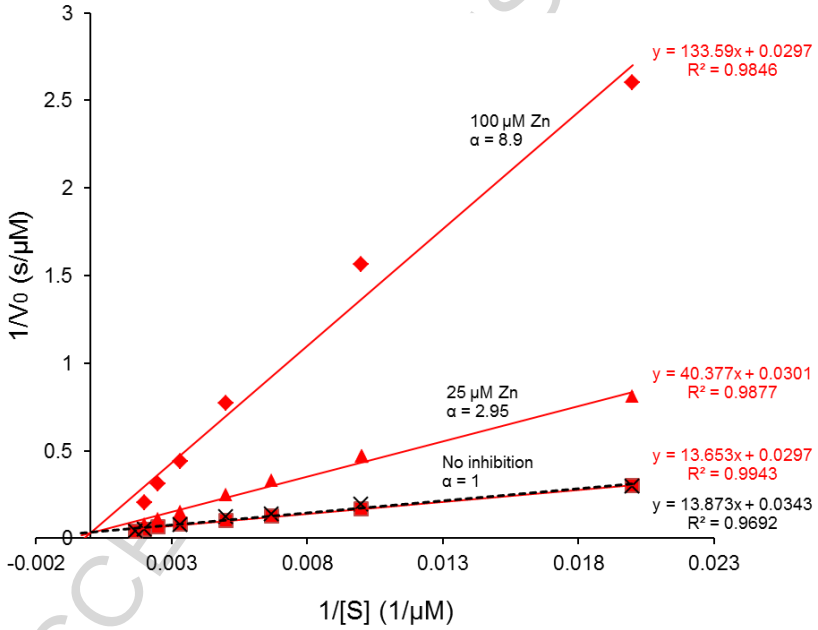

Figure 6.

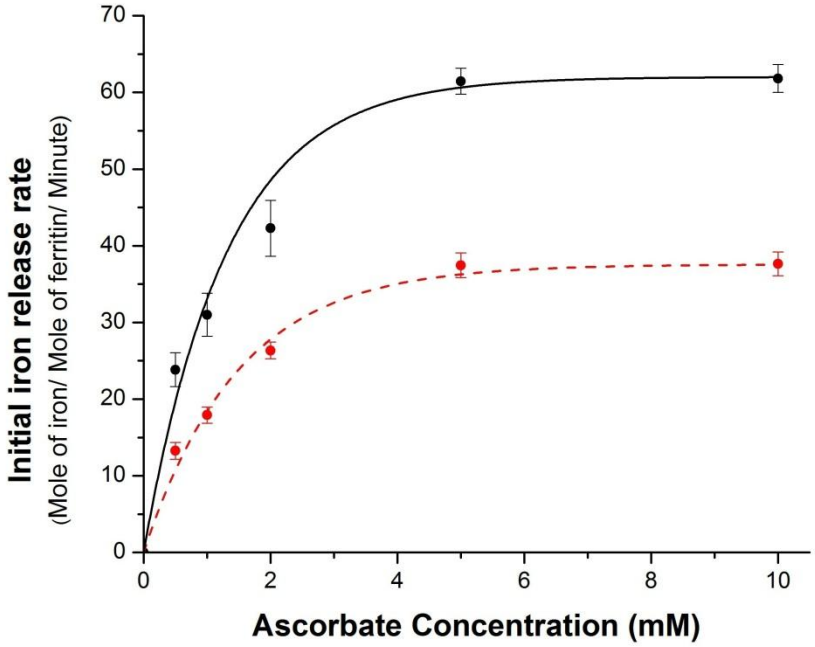

Figure 7.

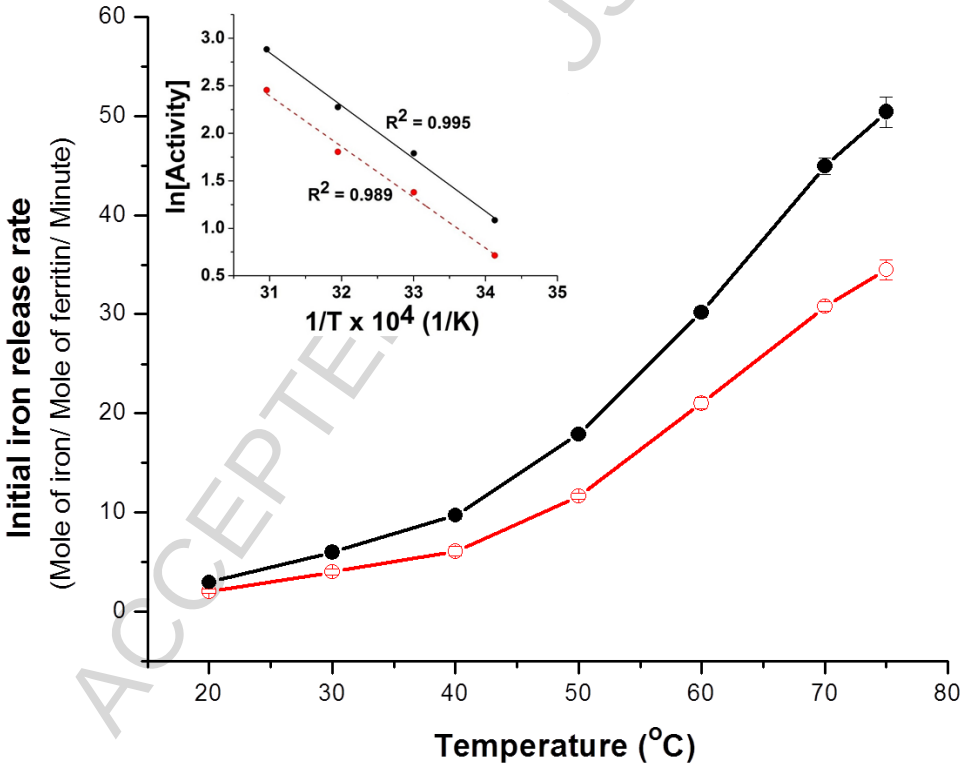

HIGHLIGHTS

- Iron binding triggers the self-assembly of *A. fulgidus* ferritin cage and its mutant
- Iron binding kinetics of the mutant AfFtn-AA is identical to the wild-type AfFtn
- Both ferritin cages, AfFtn and AfFtn-AA, disassemble upon reduction of Fe^{3+} core
- Reductive iron release of the closed mutant is slower than that of open-pore AfFtn
- The iron release rate can be controlled by varying ascorbate concentrations